STIFFNESS AND DYNAMIC ANALYSIS OF A PLANAR CLASS-2 TENSEGRITY MECHANISM

Zhifei Ji, Tuanjie Li and Min Lin
School of Electro-Mechanical Engineering, Xidian University, Xi'an, China
E-mail: zfji18@163.com; tjli888@126.com; structmlin@163.com

Received December 2013, Accepted September 2014
No. 13-CSME-201, E.I.C. Accession 3659

ABSTRACT
Tensegrity mechanisms have several attractive characteristics such as light-weight, deployable and easily modeled. In this paper, the stiffness and dynamics of a planar class-2 tensegrity mechanism are studied. Firstly, the solutions to the kinematic problems are found by using a method of reduced coordinates. Then, the stiffness of the mechanism is investigated on the basis of a stiffness matrix. The mechanism's stiffnesses along directions defined nodal coordinates are computed. Finally, a dynamic model is derived and the motions of the mechanism are simulated.

Keywords: dynamic model; kinematic model; tensegrity.

ANALYSE DE LA RAIDEUR ET DE LA DYNAMIQUE D'UN MÉCANISME PLANAIRE DE TENSÉGRITÉ DE TYPE 2

RÉSUMÉ
Les mécanismes de tenségrité ont plusieurs caractéristiques intéressantes telles que leur poids léger, une capacité de développement et une facilité de modélisation. Cet article analyse la raideur et la dynamique d'un mécanisme planaire de tenségrité de type 2. D'abord, on trouve la solution aux problèmes de cinétique par le système de coordonnées ; puis on analyse la raideur du mécanisme basée sur la raideur de la matrice. Ensuite, on calcule la cinétique de la cinématique dans le système à axe. Finalement, les mouvements du mécanisme sont simulés.

Mots-clés : modèle dynamique; modèle cinématique; tenségrité.

1. INTRODUCTION

The term tensegrity was created by Fuller [1] as a combination of the words tensional and integrity. It seems that he was inspired by some novel sculptures completed by Snelson. Furthermore, the detailed review of the history of tensegrity was given by Motro [2]. Tensegrity structures are composed of a set of compressive components (rigid rods) and tensile components (springs). The use of springs leads to an important reduction in the mass of the whole structures. Moreover, tensegrity structures are easily modeled since all the components (rigid rods and springs) are axially loaded. Due to these characteristics, tensegrity structures have been widely applied in space applications [3–5]. However, when some components (rigid rods or springs) are actuated, tensegrity systems can be applied as mechanisms. In the past twenty years, several tensegrity mechanisms have been proposed [6–9]. Furthermore, the proposed applications of tensegrity mechanisms range from a flight simulator [10], a robot [11], and a space telescope [12] to a sensor [13].

The computation of the equilibrium shape of a simple unactuated tensegrity mechanism is not an easy task for a given set of physical characteristics. The process of finding the static configurations of an unactuated tensegrity mechanism is known as form-finding. Several form finding methods are available [14, 15]. Furthermore, a method of reduced coordinates was proposed by Sultan and Corless [16] to reduce the size of the prestressability conditions of tensegrity systems. The method was used by Arsenault and Gosselin [9] to solve the kinematic problems of a planar class-1 tensegrity mechanism. The method was also used in this work to find the analytical solutions to the forward and inverse kinematic problems of a class-2 tensegrity mechanism due to its convenient physical interpretation.

During the past twenty years, considerable research has been performed on the control, statics and dynamics of class-1 tensegrity mechanisms. However, there are few articles relating to class-2 tensegrity mechanisms, especially on the study of them. In a previous work [17], the kinematics, singularities and workspaces of a planar class-2 tensegrity mechanism were researched. However, when a class-2 tensegrity mechanism is put to use, the stiffness and dynamics need to be considered. In this work, by using a stiffness matrix, the stiffness of a planar class-2 tensegrity mechanism was researched. Moreover, the dynamic model was developed using the Lagrangian method.

2. MECHANISM DESCRIPTION

A diagram of the planar class-2 tensegrity mechanism is shown in Fig. 1. It consists of four compressive components joining node pairs AE, CE, BD and BD and four tensile components joining node pairs EF, BE, DE and CD. The prismatic actuators are used to vary the distances between node pairs AB and BC. It is also noted that the mechanism's components have been numbered sequentially and have each assigned a unit vector $\mathbf{n}_i$ $(i = 1, 2, \ldots, 10)$ to define their direction. From Fig. 1, it can be seen that node A is fixed to the ground. Nodes B and C are allowed to translate without friction along the X axis while node F is allowed to translate without friction along the Y axis. The angle between the X axis and the rigid rod joining nodes A and E is defined as α while the angle between the X axis and the rigid rod joining nodes B and D is defined as β. Moreover, in Fig. 1, it should be noted that the components are connected to each other at each node by 2-d rotational joints with frictionless and the whole mechanism lies in a horizontal plane. The rigid rods are of length L. The actuator lengths, denoted by ρ_1 and ρ_2, are chosen as the mechanism's input variables while the position of node D, expressed by x and y, is chosen as the mechanism's output. Moreover, node D can be viewed as the end-effector of the mechanism. Furthermore, it is assumed that the springs are linear with k_j $(j = 1, 2, 3, 4)$, and zero free lengths. The last hypothesis is not problematic since, as was explained by Gosselin [18] and Shekarforoush et al. [19], virtual zero-free-length spring can be created by extending the actual spring beyond its attachment point. Moreover, in this work, the ranges imposed on α and β are chosen to be $0 \leq \alpha \leq \pi/2, 0 \leq \beta \leq \pi/2$. For the mechanism, it is found that when the lengths of the actuators are zero, the whole mechanism will be folded with all the nodes located on the

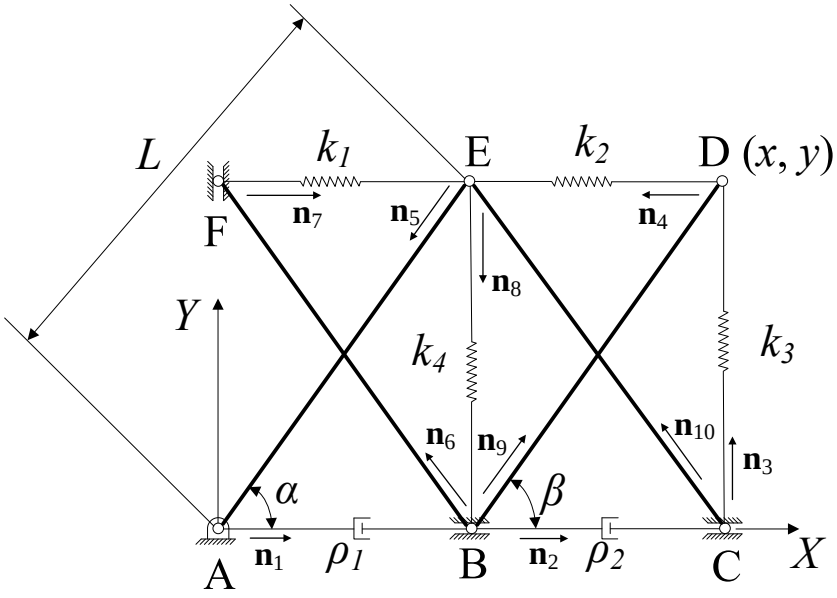

Fig. 1. Planar class-2 tensegrity mechanism.

Y axis. Moreover, by actuating the actuators, the mechanism can be erected into space. Due to this nature, the mechanism can be possible to be used as a large-scale space antenna deployable truss.

From Fig. 1, it can be observed that the position of the node D can be determined for the given actuator lengths when the mechanism is in equilibrium. Therefore, it is proper to say that the mechanism has two degrees of freedom when it is in equilibrium. In fact, when the mechanism is not in an equilibrium configuration, it actually has three degrees of freedom. Since this paper mainly discusses the kinematics and statics of the mechanism, it is always assumed that the mechanism is in equilibrium.

3. KINEMATIC ANALYSIS

3.1. Forward Kinematic Problem

For the mechanism, the forward kinematic problem (FKP) corresponds to the computation the Cartesian coordinates of node D for the given actuator lengths. According to the method of reduced coordinates [16], the equilibrium configuration of the mechanism can be found by minimizing the potential energy with respect to a minimal number of parameters representing the shape of the mechanism. From Fig. 3, it can be observed that the movement of node D is confined to a circle centered on node B with actuators locked. Therefore, only one parameter representing the shape of the mechanism, chosen here as β, is required.

As shown in Fig. 1, a cosine law for the triangle formed by nodes A, C and E can be written as follows.

$$\cos\alpha = \frac{\rho_1 + \rho_2}{2L}. \tag{1}$$

Considering the range imposed to α, the expression for $\sin\alpha$ is $\sin\alpha = \sqrt{1-\cos^2\alpha}$. Moreover, the coordinates of nodes B, C, D, E, and F can be computed.

$$\mathbf{P} = \begin{bmatrix} \rho_1 \\ 0 \end{bmatrix}, \quad \mathbf{P} = \begin{bmatrix} \rho_1 + \rho_2 \\ 0 \end{bmatrix}, \quad \mathbf{P}_E = \begin{bmatrix} L\cos\alpha \\ L\sin\alpha \end{bmatrix}, \quad \mathbf{P}_F = \begin{bmatrix} o \\ \sqrt{L^2 - \rho_1^2} \end{bmatrix}. \tag{2}$$

Since the coordinates of node D are chosen as the output variables of the mechanism, we have

$$x = \rho_1 + L\cos\beta, \tag{3}$$

$$y = L\sin\beta. \tag{4}$$

In Fig. 1, the length of the component corresponding to the vector $\mathbf{n}_i$ is denoted by L_i. With the coordinates of nodes B, C, D, E and F now known, the lengths of the components of the mechanism can be computed easily. For latter use, these lengths are provided as follows:

$$L_1 = \rho_1, \quad L_2 = \rho_2, \quad L_3 = \sqrt{\rho_2^2 + L^2 - 2\rho_2 L\cos\beta}, \tag{5}$$

$$L_4 = \sqrt{(\rho_1 + L\cos\beta - L\cos\alpha)^2 + (L\sin\beta - L\sin\alpha)^2}, \tag{6}$$

$$L_5 = L_6 = L, \quad L_7 = \sqrt{2L^2 - \rho_1^2 - 2L\sqrt{L^2 - \rho_1^2}}, \tag{7}$$

$$L_8 = \sqrt{L^2 + \rho_1^2 - 2\rho_1 L\cos\alpha}, \quad L_9 = L_{10} = L. \tag{8}$$

Furthermore, the potential energy of the mechanism can be obtained.

$$\begin{aligned} U \;=\; & \frac{2(k_1+k_2)+k_3+k_4}{2}L^2 + \frac{k_3\rho_2^2}{2} - \frac{k_1\rho_1^2}{2} - \frac{k_1\sqrt{(L^2-\rho_1^2)[4L^2-(\rho_1+\rho_2)^2]}}{2} \\ & - \frac{\rho_1\rho_2(k_2+k_4)}{2} + \frac{k_2\rho_1 - (2k_3+k_2)\rho_2}{2}L\cos\beta - \frac{\sqrt{4L^2-(\rho_1+\rho_2)^2}}{2}k_2 L\sin\beta. \end{aligned} \tag{9}$$

By differentiating the potential energy U with respect to the angle β and equating the result to zero, the following equation is generated.

$$\tan\beta = \frac{k_2\sqrt{4L^2-(\rho_1+\rho_2)^2}}{(2k_3+k_2)\rho_2 - k_2\rho_1}. \tag{10}$$

Considering the range imposed to β, computing the arctangent of Eq. (10) generates a unique solution. Moreover, by substituting this result into Eqs. (3) and (4), a solution to the forward kinematic problem is found. Especially, since the potential energy reaches its minimum when the mechanism is in equilibrium, the second derivative of U with respect to β should be always positive. From Eq. (10), it can be seen that the solution for β is independent of k_1 and k_4. This means that the springs EF and BE make no contributions to the solutions to the FKP. This case can be easily explained. From Fig. 1, it can be seen that the lengths of the springs BE and EF are determined when the actuators are locked. When this is the case, the movements of node D is constrained to a circle of radius L centered on node B and the position of node D is only dependent on the potential energy stored in the springs CD and DE. However, this is not to say that the springs BE and EF are useless. According to Knight et al. [20], the presence of the more springs (BE and EF) in mechanism allows it to be reinforced.

3.2. Inverse Kinematic Problem

The inverse kinematic problem (IKP) corresponds to the computation of the actuator lengths (ρ_1 and ρ_2) for the given coordinates (x and y) of node D. From Eqs. (3, 4), the following equations can be derived:

$$(x-\rho_1)^2 + y^2 = L^2, \tag{11}$$

$$\tan\beta = y/(x-\rho_1). \tag{12}$$

Solving Eq. (11) for ρ_1 yields

$$\rho_1 = x + \delta_1 \sqrt{L^2 - y^2}, \tag{13}$$

where $\delta_1 = \pm 1$. Generally, when $0 \leq \beta \leq \pi/2, \delta_1 = -1$. When $\pi/2 \leq \beta \leq \pi, \delta_1 = 1$. By combining Eq. (10) with (12), the following equation is generated:

$$\xi_2 \rho_2^2 + \xi_1 \rho_2 + \xi_0 = 0, \tag{14}$$

where

$$\xi_0 = k_2^2[y^2\rho_1^2 - (x-\rho_1)^2(4L^2 - \rho_1^2)], \tag{15}$$

$$\xi_1 = 2k_2\rho_1[k_2(x-\rho_1)^2 - (2k_3 + k_2)y^2], \tag{16}$$

$$\xi_2 = y^2(2k_3 + k_2)^2 + k_2^2(x-\rho_1)^2. \tag{17}$$

Solving Eq. (14) for ρ_2, we obtain

$$\rho_2 = \frac{1}{2\xi_2}[-\xi_1 + \delta_2\sqrt{\xi_1^2 - 4\xi_2\xi_0}], \tag{18}$$

where $\delta_2 = \pm 1$. From Eq. (18), two solutions for ρ_2 can be obtained. Furthermore, considering the two solutions for ρ_1 given by Eq. (13), four solutions to the inverse kinematic analysis are found.

In Section 3, the analytical relationships between the input variables (ρ_1 and ρ_2) and the output variables (x and y) are developed. These relationships are of great significance during the design and use of the mechanism. From Eqs. (13–18), it can also observed that the solutions to the IPK are independent of the springs BE and EF.

4. STIFFNESS ANLAYSIS

4.1. Stiffness Matrix

As explained by [21], a tensegrity system is composed of compressive components and tensile components. These components are all axially loaded. Since the mechanism considered here lies in a horizontal plane, its weight can thus be neglected. Due to this nature, the stiffness matrix described by Guest [22] and Arsenault [23] can be used here to analyze the stiffness of the planar class-2 tensegrity mechanism.

For a general planar tensegrity mechanism composed of n components, its configuration can be expressed by the coordinates of the nodal positions. Let m be the number of nodes in the mechanism, the vector of nodal coordinates can be defined as $\mathbf{x} = [x_1, x_2, \ldots, x_{2m}]^T$. Moreover, the corresponding external forces applied on the mechanism's nodes are defined as $\mathbf{f} = [f_1, f_2, \ldots, f_{2m}]^T$. As a consequence, the stiffness $\mathbf{K}$ relates a set of infinitesimal changes of the external forces $\delta\mathbf{f}$ to corresponding infinitesimal changes of nodal coordinates $\delta\mathbf{x}$ as follows

$$\delta\mathbf{f} = \mathbf{K}\delta\mathbf{x}. \tag{19}$$

According to [22], by differentiating the static equilibrium equations at the mechanism's nodes with respect to nodal positions, $\mathbf{K}$ can be rewritten as

$$\mathbf{K} = \mathbf{A}\hat{\mathbf{G}}\mathbf{A}^T + \mathbf{S} \tag{20}$$

In Eq. (20), $\mathbf{A}$ is the mechanism's equilibrium matrix which establishes the relationship between the external forces and the forces of the mechanism's components. Let $\mathbf{t} = [t_1, t_2, \ldots, t_n]^T$ be the forces in the components, the following equation can be obtained:

$$\mathbf{A}\mathbf{t} = \mathbf{f}. \tag{21}$$

$\hat{\mathbf{G}}$ is a diagonal matrix of modified axial stiffnesses, with an entry for each component i

$$\hat{g}_i = g_i - \hat{t}_i, \tag{22}$$

where g_i is the conventional axial stiffness of the component and $\hat{t}_i = t_i/L_i$ is its tension coefficient. Finally, $\mathbf{S}$ is the mechanism's stress matrix. $\mathbf{S}$ can be written as the Kronecker product of a small or reduced stress matrix Ω and a 2-dimensional identify matrix $\mathbf{I}$.

$$\mathbf{S} = \Omega \otimes \mathbf{I}, \tag{23}$$

where

$$\Omega_{ij} = \begin{cases} -\hat{t}_{i,j} = -\hat{t}_{j,i} & \text{if} \quad i \neq j, \quad \text{and} \quad \{i,j\}\text{a member} \\ \sum_{k \neq i} \hat{t}_{ik} & \text{if} \quad i = j \\ 0 & \text{if there is no connection between node } i \text{ and node } j. \end{cases} \tag{24}$$

In Eq. (24), $\hat{t}_{i,j}$ is the tension coefficient in the member that runs between nodes i and j.

4.2. Computation of the Stiffness Matrix

From Eq. (20), it can be seen that in order to compute the stiffness matrix $\mathbf{K}$, the equilibrium matrix $\mathbf{A}$, modified axial stiffness matrix $\hat{\mathbf{G}}$ and the stress matrix $\mathbf{S}$ should be computed firstly.

4.2.1. Computation of the equilibrium matrix

For the mechanism studied here, the vector of generalized coordinates used to represent the mechanism's configuration can be expressed as

$$\mathbf{x} = [a_{Ax}, a_{Bx}, a_{By}, a_{Cx}, a_{Cy}, a_{Dx}, a_{Dy}, a_{Ex}, a_{Ey}, a_{Fx}, a_{F_y}]^T, \tag{25}$$

where a_{Px} and a_{Py} represent the X and Y coordinates of nodes P respectively $(P \in \{A,B,C,D,E,F\})$. Meanwhile, a corresponding vector of external forces applied to the nodes is defined as

$$\mathbf{f} = [f_{Ax}, f_{Ay}, f_{Bx}, f_{By}, f_{Cx}, f_{Cy}, f_{Dx}, f_{Dy}, f_{Ex}, f_{Ey}, f_{Fx}, f_{Fy}]^T, \tag{26}$$

where f_{Px} and f_{Py} are the components along the X and Y axes of the external force applied to node P. From Fig. 1, it can be seen that there are ten components corresponding to vectors $\mathbf{n}_i$ in the mechanism. The vector of tension forces in the components is thus expressed as

$$\mathbf{t} = [t_1, t_2, t_3, t_4, t_5, t_6, t_7, t_8, t_9, t_{10}]^T \tag{27}$$

By writing the equilibrium equations at each node of the mechanism and manipulating them in the form of Eq. (21), the equilibrium matrix $\mathbf{A}$ is given by

$$\mathbf{A} = \begin{bmatrix} \mathbf{n}_1 & \mathbf{0} & \mathbf{0} & \mathbf{0} & -\mathbf{n}_5 & \mathbf{0} & \mathbf{0} & \mathbf{0} & \mathbf{0} & \mathbf{0} \\ -\mathbf{n}_1 & \mathbf{n}_2 & \mathbf{0} & \mathbf{0} & \mathbf{0} & \mathbf{n}_6 & \mathbf{0} & -\mathbf{n}_8 & \mathbf{n}_9 & \mathbf{0} \\ \mathbf{0} & -\mathbf{n}_2 & \mathbf{n}_3 & \mathbf{0} & \mathbf{0} & \mathbf{0} & \mathbf{0} & \mathbf{0} & \mathbf{0} & \mathbf{n}_{10} \\ \mathbf{0} & \mathbf{0} & -\mathbf{n}_3 & \mathbf{n}_4 & \mathbf{0} & \mathbf{0} & \mathbf{0} & \mathbf{0} & -\mathbf{n}_9 & \mathbf{0} \\ \mathbf{0} & \mathbf{0} & \mathbf{0} & -\mathbf{n}_4 & \mathbf{n}_5 & \mathbf{0} & -\mathbf{n}_7 & \mathbf{n}_8 & \mathbf{0} & \mathbf{n}_{10} \\ \mathbf{0} & \mathbf{0} & \mathbf{0} & \mathbf{0} & \mathbf{0} & -\mathbf{n}_6 & \mathbf{n}_7 & \mathbf{0} & \mathbf{0} & \mathbf{0} \end{bmatrix}, \tag{28}$$

where $\mathbf{0}$ is a two-dimensional zero vector. As stated in Section 2, node A is fixed to the ground. The X and Y coordinates of node A are always equal to zero. This means that the stiffnesses of the mechanism along

a_{Ax} and a_{Ay} are infinite. Due to this fact, the scale of matrix A can be reduced. From Fig. 1, the constraints of the mechanism can be observed as

$$a_{Ax} = a_{Fx} = 0, \quad a_{Ay} = a_{By} = a_{Cy} = 0. \tag{29}$$

Taking into account Eq. (29), the vectors of nodal coordinates and external forces are firstly reduced into the following forms.

$$\mathbf{x}_r = [a_{Bx}, a_{Cx}, a_{Dx}, a_{Dy}, a_{Ex}, a_{Ex}, a_{Ey}, a_{Fy}]^T, \tag{30}$$

$$\mathbf{F}_r = [f_{Bx}, f_{Cx}, f_{Dx}, f_{Dy}, f_{Ex}, f_{Ey}, f_{Fy}]^T. \tag{31}$$

By removing the rows corresponding to $f_{Ax}, f_{Ay}, f_{By}, f_{Cy}$ and f_{Fx}, the equilibrium matrix $\mathbf{A}$ becomes

$$\mathbf{A}_r = \begin{bmatrix} -n_{1x} & n_{2x} & 0 & 0 & 0 & n_{6x} & 0 & -n_{8x} & n_{9x} & 0 \\ 0 & -n_{2x} & n_{3x} & 0 & 0 & 0 & 0 & 0 & 0 & \mathbf{n}_{10x} \\ 0 & 0 & -\mathbf{n}_3 & \mathbf{n}_4 & 0 & 0 & 0 & 0 & -\mathbf{n}_9 & 0 \\ 0 & 0 & 0 & -\mathbf{n}_4 & \mathbf{n}_5 & 0 & -\mathbf{n}_7 & \mathbf{n}_8 & 0 & -\mathbf{n}_{10} \\ 0 & 0 & 0 & 0 & 0 & -n_{6y} & n_{7y} & 0 & 0 & 0 \end{bmatrix}, \tag{32}$$

where

$$\mathbf{A}_r \mathbf{t}_r = \mathbf{f}_r \tag{33}$$

4.2.2. Computation of the modified axial stiffness matrix

Referring to Eq. (22), it is seen that the modified axial stiffness of a component depends on its axial stiffness g_i as well as its tension coefficient $\hat{t}_i$. For springs, g_i is equal to k_i. For struts, g_i depends on the material properties. In this paper, the struts are assumed to have the same axial stiffness k_b while the actuators are assumed to have the same axial stiffness k_a. In order to compute the forces in the struts and actuators, Eq. (33) is rewritten as

$$t_3 \mathbf{a}_{r_3} + t_4 \mathbf{a}_{R_4} + t_7 \mathbf{a}_{r_7} + \mathbf{A}_0 \mathbf{t}_0 = \mathbf{f}_r, \tag{34}$$

where $\mathbf{A}_0 = [\mathbf{a}_{r1} \;\; \mathbf{a}_{r2} \;\; \mathbf{a}_{r5} \;\; \mathbf{a}_{r6} \;\; \mathbf{a}_{r8} \;\; \mathbf{a}_{r9} \;\; \mathbf{a}_{r10}]$ with $\mathbf{a}_{ri}$ being the ith column of $\mathbf{A}_r$. $\mathbf{t}_0$ is equal to $\mathbf{t}_r$ with the rows corresponding to t_3, t_4 and t_7 removed. Solving Eq. (34) for $\mathbf{t}_0$ yields

$$\mathbf{t}_0 = \mathbf{A}_0^{-1}(\mathbf{f}_r - t_3 \mathbf{a}_{r_3} - t_4 \mathbf{a}_{r_4} - t_7 \mathbf{a}_{r_7}). \tag{35}$$

Using the solutions to the IKP (see Section 3.2), the lengths of the components of the mechanism can be computed by Eqs. (5–8). Then, the forces in the springs can thus be obtained. Substituting there results into Eq. (35), the forces in the struts and actuators can be arrived at. With the forces and lengths of all the components computed, the tension coefficient $\hat{t}_i$ can be determined. Therefore, the matrix $\hat{\mathbf{G}}$ takes the following form:

$$\begin{aligned} \hat{\mathbf{G}} \;=\; \text{Diag} \Bigg(& k_a - \frac{t_1}{L_1} \;\; k_a - \frac{t_2}{L_2} \;\; k_3 - \frac{t_3}{L_3} \;\; k_2 - \frac{t_4}{L_4} \;\; k_b - \frac{t_5}{L_5} \;\; k_b - \frac{t_6}{L_6} \\ & k_1 - \frac{t_7}{L_7} \;\; k_4 - \frac{t_8}{L_8} \;\; k_b - \frac{t_9}{L_9} \;\; k_b - \frac{t_{10}}{L_{10}} \Bigg) \end{aligned} \tag{36}$$

4.2.3. Computation of the stress matrix

According to Eq. (23), the stress matrix of the mechanism is found as

$$\mathbf{S} = \begin{bmatrix} \zeta_1\mathbf{1}_d & -\hat{t}_1\mathbf{1}_d & 0 & 0 & -\hat{t}_5\mathbf{1}_d & 0 \\ -\hat{t}_1\mathbf{1}_d & \zeta_2\mathbf{1}_d & -\hat{t}_2\mathbf{1}_d & -\hat{t}_9\mathbf{1}_d & -\hat{t}_8\mathbf{1}_d & -\hat{t}_6\mathbf{1}_d \\ 0 & -\hat{t}_2\mathbf{1}_d & \zeta_3\mathbf{1}_d & -\hat{t}_3\mathbf{1}_d & -\hat{t}_{10}\mathbf{1}_d & 0 \\ 0 & -\hat{t}_9\mathbf{1}_d & -\hat{t}_3\mathbf{1}_d & \zeta_4\mathbf{1}_d & -\hat{t}_4\mathbf{1}_d & 0 \\ -\hat{t}_5\mathbf{1}_d & -\hat{t}_8\mathbf{1}_d & -\hat{t}_{10}\mathbf{1}_d & -\hat{t}_4\mathbf{1}_d & \zeta_5\mathbf{1}_d & -\hat{t}_7\mathbf{1}_d \\ 0 & -\hat{t}_6\mathbf{1}_d & 0 & 0 & -\hat{t}_7\mathbf{1}_d & \zeta_6\mathbf{1}_d \end{bmatrix} \tag{37}$$

where

$$\begin{aligned} \zeta_1 &= \hat{t}_1+\hat{t}_5, \quad \zeta_2 = \hat{t}_1+\hat{t}_2+\hat{t}_6+\hat{t}_8+\hat{t}_9, \quad \zeta_3 = \hat{t}_2+\hat{t}_3+\hat{t}_{10} \\ \zeta_4 &= \hat{t}_3+\hat{t}_4+\hat{t}_9, \quad \zeta_5 = \hat{t}_4+\hat{t}_5+\hat{t}_7+\hat{t}_8+\hat{t}_{10}, \quad \zeta_6 = \hat{t}_6+\hat{t}_7. \end{aligned} \tag{38}$$

This matrix can be reduced by taking into account the constraints expressed by Eq. (29). This is done by deleting the first, second, forth, sixth and eleventh rows of the matrix $\mathbf{S}$. Moreover, the reduced stress matrix is given by

$$\mathbf{S}_r = \begin{bmatrix} \zeta_2 & -\hat{t}_2 & -\hat{t}_9 & 0 & -\hat{t}_8 & 0 & 0 \\ -\hat{t}_2 & \zeta_3 & -\hat{t}_3 & 0 & -\hat{t}_{10} & 0 & 0 \\ -\hat{t}_9 & -\hat{t}_3 & \zeta_4 & 0 & -\hat{t}_4 & 0 & 0 \\ 0 & 0 & 0 & \zeta_4 & 0 & -\hat{t}_4 & 0 \\ -\hat{t}_8 & -\hat{t}_{10} & -\hat{t}_4 & 0 & \zeta_5 & 0 & 0 \\ 0 & 0 & 0 & -\hat{t}_4 & 0 & \zeta_5 & -\hat{t}_7 \\ 0 & 0 & 0 & 0 & 0 & -\hat{t}_7 & \zeta_6 \end{bmatrix}. \tag{39}$$

With matrices $\mathbf{A}_r, \hat{\mathbf{G}}$ and $\mathbf{S}_r$ now defined, the stiffness matrix for the mechanism of interest can be computed, referring to Eq. (20), as

$$\mathbf{K} = \mathbf{A}_r\hat{\mathbf{G}}\mathbf{A}_r^T + \mathbf{S}_r \tag{40}$$

4.3. Stiffness along a Coordinate Direction

Generally, intuitive information of the stiffness of the mechanism can not be extracted from the stiffness matrix $\mathbf{K}$. To solve this problem, stiffness indices, computed form the stiffness matrix, are usually used to obtain the useable knowledge regarding the mechanism's stiffness. Different stiffness indices and their computations were introduced in [22, 23]. Here, the stiffnesses of the mechanism along the directions defined by nodal coordinates were discussed. From Eq. (19), it can be seen that the stiffness matrix establishes a relationship between infinitesimal forces applied in the directions of the nodal coordinates and the corresponding changes in these coordinates. Similarly, the stiffness along a direction x_i is defined as $\delta f_i = K_i\delta x_i$. To compute K_i, Eq. (19) can be broken down as follows [23]:

$$\delta f_i = \mathbf{u}_i\delta\mathbf{x}_{r_i} + K_{ii}\delta x_i, \tag{41}$$

$$\delta\mathbf{f}_{r_i} = \mathbf{K}_{r_i}\delta\mathbf{x}_{r_i} + \mathbf{v}_i\delta x_i, \tag{42}$$

where K_{r_i} is the matrix $\mathbf{K}$ with the ith row and column removed, $\mathbf{u}_i$ is the ith row of $\mathbf{K}$ with the ith element removed, $\mathbf{v}_i$ is the ith column of $\mathbf{K}$ with the ith element removed, K_{ii} is the element on the ith row and column of $\mathbf{K}, \delta\mathbf{x}_{r_i}$ is the vector $\delta\mathbf{x}$ with the ith element removed, and $\delta\mathbf{f}_{r_i}$ is the vector $\delta\mathbf{f}$ with the ith element removed. In order to find the relationship between δf_i and δx_i, it is assumed that infinitesimal

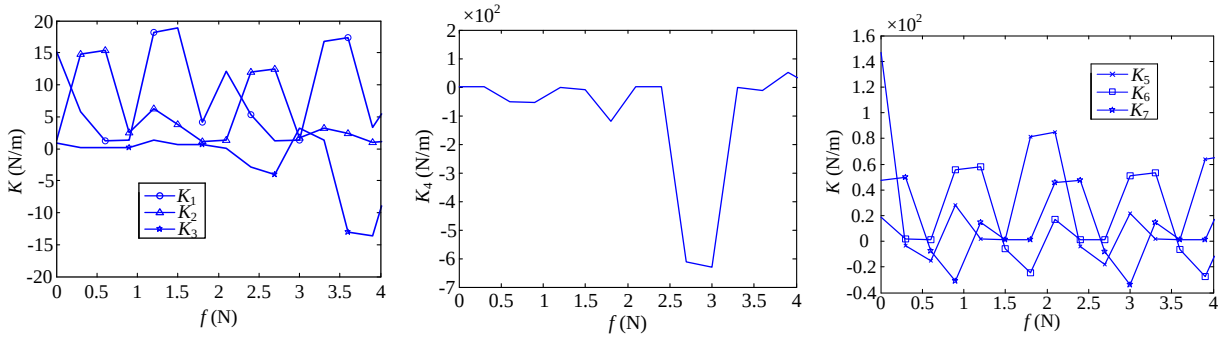

Fig. 2. Stiffness of the mechanism along generalized coordinates: (a) stiffness along a_{Bx}, a_{Cx} and a_{Dx}; (b) stiffness along a_{Dy}; (c) stiffness along a_{Ex}, a_{Ey} and a_{Fy}.

forces are only applied along the direction defined by x_i. This means that $\delta \mathbf{f}_{r_i} = 0$. By combining Eq. (41) with Eq. (42), the stiffness K_i can be obtained:

$$K_i = K_{ii} - \mathbf{u}_i \mathbf{K}_{r_i}^{-1} \mathbf{v}_i. \tag{43}$$

Oppenheim and Williams [24] developed the force-displacement relationship of a symmetrical tensegrity structure at different values of pre-stress by using an energy approach. The developed force-displacement relationship is benefit from the symmetry of the tensegrity structure. For a tensegrity system of arbitrary shape, the stiffness matrix is more proper to analyze the system's stiffness. Moreover, applying this method to the mechanism of interest, the stiffness along nodal coordinates can be computed. From Fig. 1, it can be seen that the pre-stress can be adjusted by applying an external force f on node F along Y axis. Here, it is interesting to investigate the variation of the stiffness of the mechanism along nodal coordinates with respect to the external force f. This can be done by setting the vector expressed by Eq. (31) as

$$\mathbf{f}_r = [0,0,0,0,0,0,f]^T. \tag{44}$$

By substituting Eq. (44) into Eq. (35), $\mathbf{t}_0$ is obtained. Subsequently, $\hat{\mathbf{G}}$ and $\mathbf{S}_r$ can thus be computed. Substituting these results into Eq. (43), the relationship between K_i and f can be obtained. The plots of K_i as a function of f are shown in Fig. 2 with $k_1 = k_2 = k_3 = k_4 = 1, k_a = 10$ and $k_b = 1000$. It is noted that K_i is the stiffness along the ith coordinate in Eq. (30).

From Fig. 2(a–c), it can be seen that the stiffness of the mechanism along nodal coordinates varies considerably with respect to the external force f. If $f = 0$, the stiffnesses K_2, K_3 and K_4 are near zero. When this is the case, the mechanism almost does not have the ability to resist the forces along directions defined by a_{Cx}, a_{Dx} and a_{Dy}. Moreover, when $f \in [2 \;\; 3.5]$, the stiffness K_4 varies rapidly. This fact needs to be considered during the design and use of the mechanism.

5. DYNAMIC ANALYSIS

In Section 3, the solutions to the FKP and IKP are found by using an energy formulation. However, these solutions are not valid when the mechanism is not in equilibrium. Therefore, it is useful to investigate the mechanism's dynamics in order to gain knowledge on its behavior when the mechanism is moving from one equilibrium configuration to another.

5.1. Hypotheses

In order to derive an appropriate dynamic model of the mechanism, the following hypotheses are made:

- Each strut is modeled as a thin rod of mass m and of moment of inertia $I = mL^2/12$ (about an axis perpendicular to the plane and passing through the strut's centroid).
- The springs are massless and linear damped with coefficients c_1, c_2, c_3 and c_4.
- The actuators are massless.

5.2. Equations of Motion

As stated in Section 2, the mechanism has two degrees of freedom since the position of node D is controlled by modifying the lengths of two actuators. However, when the mechanism is not in equilibrium, it actually has three degrees of freedom. For this reason, three generalized coordinates, chosen as ρ_1, ρ_2 and β, are needed to develop the dynamic model.

The Lagrangian approach has been used quite frequently for the dynamic modeling of tensegrity systems. Here, this method is also used to develop the dynamic model of the class-2 tensegrity mechanism. The motion equations of the mechanism can be written by

$$\frac{d}{dt}\frac{\partial T}{\partial \dot{\mathbf{q}}} - \frac{\partial T}{\partial \mathbf{q}} + \frac{\partial U}{\partial \mathbf{q}} = \mathbf{f}_e \tag{45}$$

where T and U are the kinetic and potential energies of the mechanism, $\mathbf{q} = [\rho_1, \rho_2, \beta]^T$ is the vector of generalized coordinates and $\mathbf{f}_e = [f_{e_1}, f_{e_2}, f_{e_3}]^T$ is the vector of non-conservative forces acting on the system. The kinetic energy, due only to the movements of the struts, can be expressed as

$$\begin{aligned} T \;=\; & \frac{m}{8}\Bigg\{(\dot{\rho}_1 + \dot{\rho}_2 - L\sin\alpha\,\dot{\alpha})^2 + (\cos^2\alpha + 1)L^2\dot{\alpha}^2 + \left(4 + \frac{L^2}{L^2 - \rho_1^2}\right)\dot{\rho}_1^2 + L^2\dot{\beta}^2 \\ & - 4L\dot{\rho}_1\dot{\beta}\sin\beta\Big\} + \frac{I}{2}\left\{2\dot{\alpha}^2 + \dot{\beta}^2 + \frac{\dot{\rho}_1^2}{L^2 - \rho_1^2}\right\}\Bigg\}, \end{aligned} \tag{46}$$

where $\dot{\alpha}$ can be expressed in terms of the generalized coordinates by substituting Eq. (1) into the following:

$$\dot{\alpha} = \frac{-1}{\sqrt{1 - \cos^2\alpha}}\,\frac{d(\cos\alpha)}{dt}. \tag{47}$$

An expression for the potential energy of the mechanism has already been presented in Eq. (9). The non-conservative forces, which correspond to the damping in the springs as well as the forces in the actuators, are given by

$$f_{e_1} = -c\dot{L}_3\frac{\partial L_3}{\partial \rho_1} - c\dot{L}_4\frac{\partial L_4}{\partial \rho_1} - c\dot{L}_7\frac{\partial L_7}{\partial \rho_1} - c\dot{L}_8\frac{\partial L_8}{\partial \rho_1} - f_1, \tag{48}$$

$$f_{e_2} = -c\dot{L}_3\frac{\partial L_3}{\partial \rho_2} - c\dot{L}_4\frac{\partial L_4}{\partial \rho_2} - c\dot{L}_7\frac{\partial L_7}{\partial \rho_2} - c\dot{L}_8\frac{\partial L_8}{\partial \rho_2} - f_2, \tag{49}$$

$$f_{e_3} = -c\dot{L}_3\frac{\partial L_3}{\partial \beta} - c\dot{L}_4\frac{\partial L_4}{\partial \beta} - c\dot{L}_7\frac{\partial L_7}{\partial \beta} - c\dot{L}_8\frac{\partial L_8}{\partial \beta}, \tag{50}$$

where the expressions for L_3, L_4, L_7 and L_8 are given by Eqs. (5–8). f_1 and f_2 are the forces in the actuators. Substituting these elements in Eq. (45) yields the equations of motion of the mechanism:

$$\mathbf{M}\ddot{\mathbf{q}} + \mathbf{F}\dot{\mathbf{q}}_p + \mathbf{G}\dot{\mathbf{q}}_q + \mathbf{H}\dot{\mathbf{q}} + \mathbf{W} = 0, \tag{51}$$

where $\dot{\mathbf{q}}_p = [\dot{\rho}_1^2, \dot{\rho}_2^2, \dot{\beta}_1^2]^T$ and $\dot{\mathbf{q}}_q = [\dot{\rho}_1\dot{\rho}_2, \dot{\rho}_1\dot{\beta}, \dot{\rho}_2\dot{\beta}]^T$. Moreover, $\mathbf{M}, \mathbf{F}, \mathbf{G}$ and $\mathbf{H}$ are all 3×3 matrices. $\mathbf{W}$ is a 3×1 vector. The elements of these matrices and vectors are detailed in Appendix A.

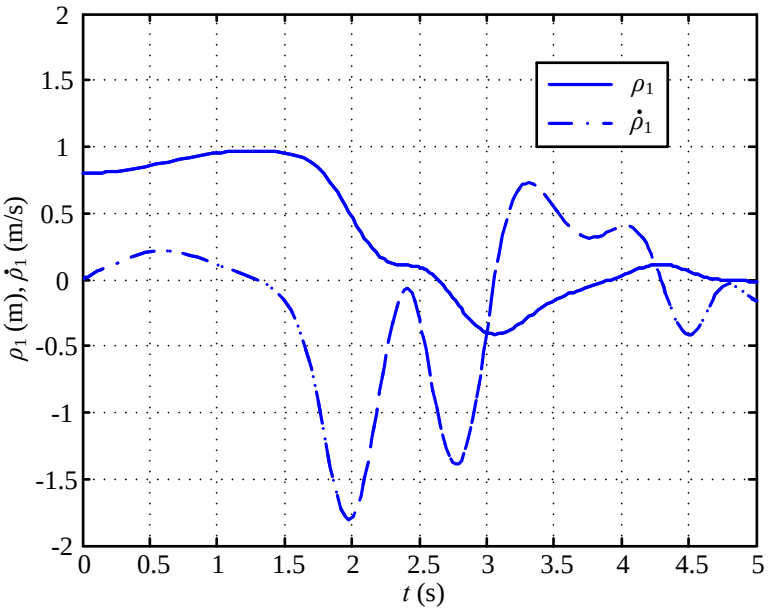

Fig. 3. Motion of the generalized coordinate ρ_1.

5.3. Simulation

In this section, the motions of the mechanism will be simulated by controlling the forces in the actuators. To complete such simulation, the initial values for the generalized coordinates should be determined first. It is assumed that the mechanism moves from an initial equilibrium configuration $\mathbf{q}_0$. The initial values of actuators are set to be $\rho_{10} = \rho_{20} = 0.7$ m. By substituting this result into Eq. (10), the initial value for β is found ($\beta_0 = 0.8$). Therefore, $\mathbf{q}_0 = [0.7 \;\; 0.7 \;\; 0.8]^T$ is selected as the initial conditions for Eq. (51). Moreover, the initial velocities of the generalized coordinates are set to be zero.

The forces in the actuators are chosen as: $f_1 = 10\rho_1 t$ and $f_2 = 10\rho_2 t$. t is the time. The parameters that were used for the mechanism are as follows:

- $k_1 = k_2 = k_3 = k_4 = 1$ N/m
- $c_1 = c_2 = c_3 = c_4 = 0.01$ N $\cdot$ s/m
- $m = 2$ kg
- $L = 1$ m

Using the Runge–Kutta method, the numeral solutions to the dynamic equations of the mechanism can be found. By solving Eq. (51), the generalized coordinates and their velocities are obtained during the motion of the mechanism, which are shown in Figs. 3–5.

From Figs. 3–5, it can be seen that the mechanism moves from $\mathbf{q}_0$ ($t = 0$ s) to $\mathbf{q}_F = [0 \;\; 0 \;\; \pi/2]$ ($t = 2.5$ s), driven by the forces in the actuators. When the mechanism reaches the configuration $\mathbf{q}_F$, the forces in the actuators are zero (since the lengths of actuators are zero). However, when $t > 2.5$ s, oscillations of the generalized coordinates do exist due to the inertia of the mechanism. After a certain period of time, such oscillations will be diminished and the mechanism will be in the equilibrium configuration $\mathbf{q}_F$. The certain period of time depends on the damping in the springs. From Fig. 1, it can be seen that the configuration $\mathbf{q}_F$ corresponds to the situation where all the nodes of the mechanism are located along the Y axis. When this

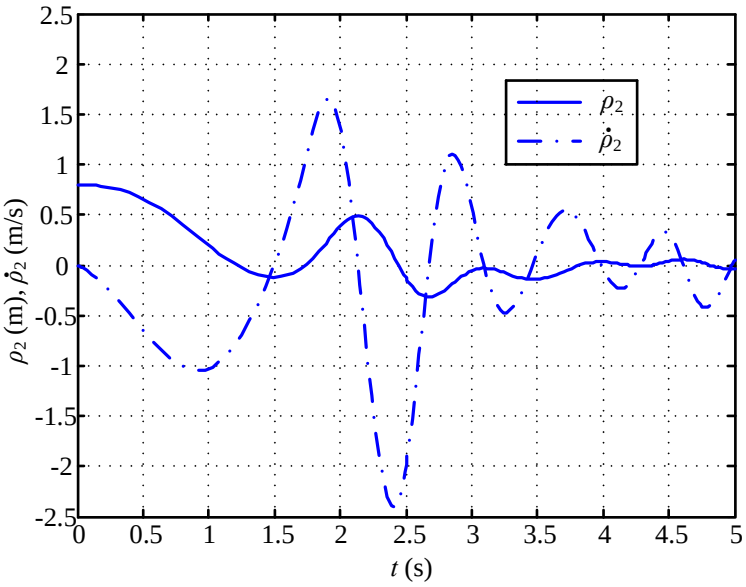

Fig. 4. Motion of the generalized coordinate ρ_2.

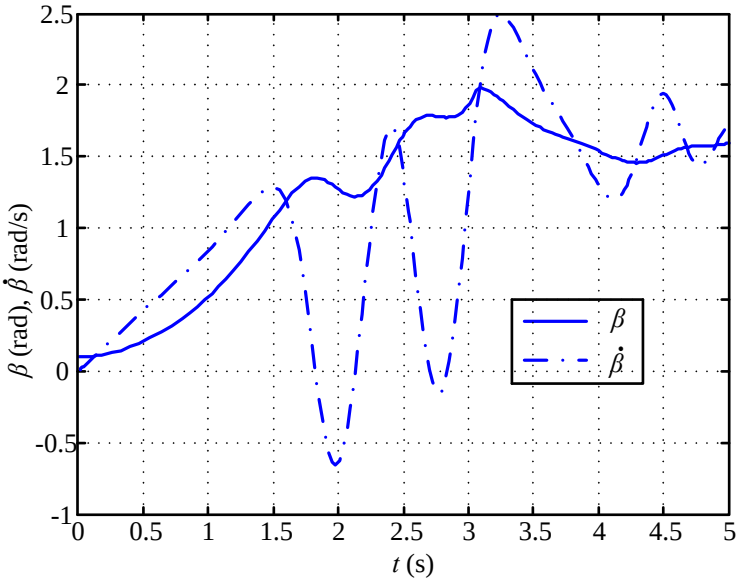

Fig. 5. Motion of angle β.

is the case, the infinitesimal movements of node D along Y axis can not be generated. Therefore, $\mathbf{q}_F$ is a singular configuration.

Here it is interesting to research the trajectory of the end-effector (node D) when the mechanism moves from $\mathbf{q}_0$ to $\mathbf{q}_F$. From Section 3, it is demonstrated that the position of the end-effector can be determined for a set of given actuator lengths when the mechanism is in equilibrium. For a certain moment t, the generalized coordinates ρ_1, ρ_2 and β are obtained by Eq. (51) (see Figs. 3–5). By substituting this result into Eqs. (3) and (4), the position of the end-effector can be defined (denoted by (x_1, y_1)). Furthermore, using the solutions to the FKP, the equilibrium position of the end-effector (denoted by (x_0, y_0)) can also be

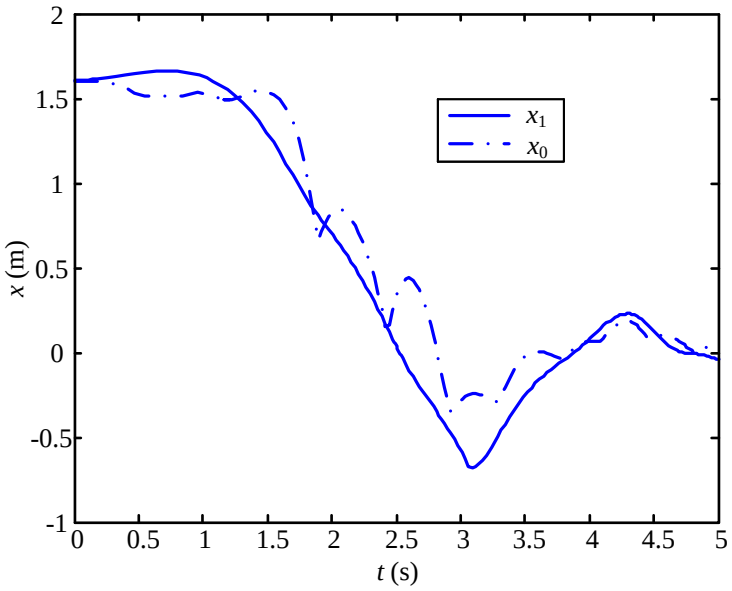

Fig. 6. X coordinate of the end-effector.

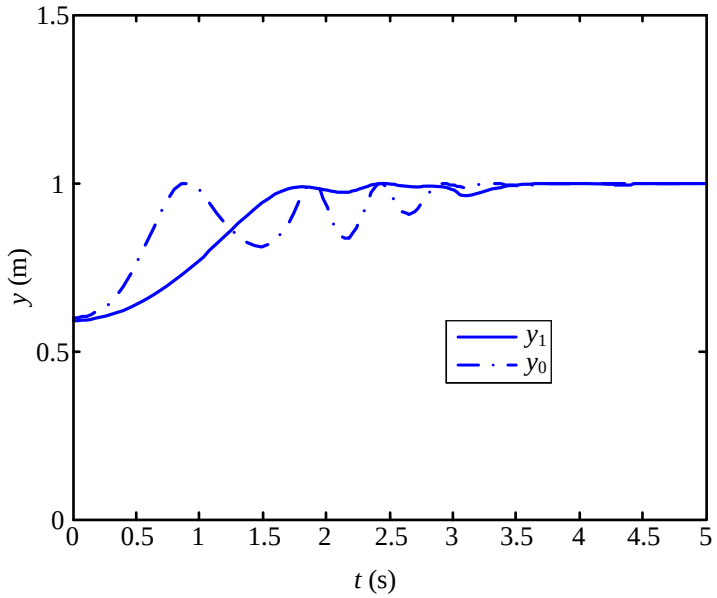

Fig. 7. Y coordinate of the end-effector.

defined for this moment t. The motion of the end-effector is expressed by its Cartesian coordinates x and y which is shown in Figs. 6–7.

From Figs. 6 and 7 it can be seen that the relationship of the lengths of the actuators and coordinates of the end-effector, developed in Section 3.1, is not valid during the motion process of the mechanism. This is due to the fact that when the mechanism generates motions, the constraint that the mechanism's potential energy is at its minimum does not exist. This is why the kinematics and statics of the class-2 tensegirty mechanism should be considered simultaneously. This nature brings difficulties to the control and path planning for

such mechanisms since explicit relationships between the input and ouput does not exist. Moreover, this fact needs to be considered during the design and use of the mechanism.

6. CONCLUSION

An adaptive method of reduced coordinates was employed in this paper to find the analytical solutions to the forward and inverse kinematic problems. According to the method of reduced coordinates, the equilibrium configurations can be obtained by minimizing the potential energy with respect to a minimal number of parameters representing the shape of the mechanism. Afterwards, the relationship between the external load and the corresponding deformations was developed by the stiffness matrix. The stiffnesses of the mechanism along directions defined by nodal coordinates were computed. Finally, using the Lagrangian approach, the dynamic model of the mechanism was developed and simulated. It is found that unlike conventional mechanisms, the class 2 tensegrity mechanism obtained one more degree of freedom when it is not in equilibrium. The solutions to the forward kinematic problems are not valid when the mechanism is in movement. This nature brings difficulties for the control and path planning for such mechanism. The work in this paper lays good foundation for the use and design of the mechanism.

ACKNOWLEDGEMENT

This research is supported by the National Natural Science Foundation of China (No. 51375360).

REFERENCES

1. Fuller, B., "Tensile-integrity structures", United States Patent 3,063,521, November 1962.
2. Motro, R., "Tensegrity systems: The state of the art", *International Journal of Space Structures*, Vol. 7, No. 2, pp. 75–83, 1992.
3. Korkmaz, S., Bel Hadj Ali, N. and Smith, I.F.C., "Configuration of control system for damage tolerance of a tensegrity bridge", *Advanced Engineering Informatics*, Vol. 26, No. 1, pp. 145–155, 2012.
4. Rhode-Barbarigos, L., Bel Hadj Ali, N., Motro, R. and Smith, I.F.C., "Design aspects of a deployable tensegrity-hollow-rope footbridge", *International Journal of Space Structures*, Vol. 27, No. 2, pp. 81–96, 2012.
5. Fazli, N. and Abedian A., "Design of tensegrity structures for supporting deployable mesh antennas", *Scientia Iranica*, Vol. 18, No. 5, pp. 1078–1087, 2011.
6. Mohr, C.A. and Arsenault, M., "Kinematic analysis of a translational 3-DOF tensegrity mechanism", *Transactions of the Canadian Society for Mechanical Engineering*, Vol. 35, No. 4, pp. 573–584, 2011.
7. Swartz, M.A. and Hayes, M.J.D., "Kinematic and dynamic analysis of a spatial one-DOF foldable tensegrity mechanism", *Transactions of the Canadian Society for Mechanical Engineering*, Vol. 31, No. 4, pp. 421–431, 2007.
8. Arsenault, M. and Gosselin, C.M., "Kinematic and static analysis of a 3-PUPS spatial tensegrity mechanism", *Mechanism and Machine Theory*, Vol. 44, No. 1, pp. 162–179, 2009.
9. Arsenault, M. and Gosselin, C.M., "Kinematic and dynamic analysis of a planar one-degree-of-freedom tensegrity mechanism", *Journal of Mechanical Design*, Vol. 127, No. 6, pp. 1152–1160, 2005.
10. Sultan, C. and Corless, M., "Tensegrity flight simulator", *Journal of Guidance, Control and Dynamics*, Vol. 23, No. 6, pp. 1055–1064, 2000.
11. Paul, C., Valero-Cuevas, F.J. and Lipson, H., "Design and control of tensegrity robots for locomotion", *IEEE Transactions on Robotics*, Vol. 22, No. 5, pp. 944–957, 2006.
12. Sultan, C., Corless, M. and Skelton, R.E., "Peak to peak control of an adaptive tensegrity space telescope", in *Proceedings of SPIE – The International Society for Optical Engineering (CSME) Forum*, Newport Beach, CA, USA, pp. 190–201, March 1–4, 1999.
13. Sultan, C. and Skelton, R., "A force and torque tensegrity sensor", *Sensors and Actuators A: Physical*, Vol. 112, Nos. 2–3, pp. 220–231, 2004.
14. Koohestani, K., "Form-finding of tensegrity structures via genetic algorithm", *International Journal of Solids and Structures*, Vol. 49, No. 5, pp. 739–747, 2012.

15. Tran, H.C. and Lee, J., "Form-finding of tensegrity structures using double singular value decomposition", *Engineering with Computers*, Vol. 29, No. 1, pp. 71–86, 2013.
16. Sultan, C., Corless, M. and Skelton, R.E., "Reduced prestressability coordinates for tensegrity structures", in *Proceedings of the 40th AIAA/ASME/ASCE/AHS/ASC Structures, Structural Dynamics and Materials Conference*, St Louis, MO, USA, April 12–15, pp. 2300–2308, 1999.
17. Ji, Z., Li, T. and Lin, M., "Kinematics, singularity and workspaces of a planar 4-bar tensegrity mechanism", *Journal of Robotics*, Vol. 2014, pp. 10, 2014.
18. Gosselin, C.M., "Static balancing of spherical 3-DOF parallel mechanisms and manipulators", *The International Journal of Robotics Research*, Vol. 18, No. 2, pp. 819–829, 1999.
19. Shekarforoush, S.M.M., Eghtesad, M. and Farid, M., "Design of statically balanced six-degree-of-freedom parallel mechanisms based on tensegrity system", in *2009 ASME International Mechanical Engineering Congress and Exposition*, Lake Buena Vista, FL, USA, November 13–19, pp. 245–253, 2009.
20. Knight, B., Zhang, Y., Duffy, J., Crane, C.D. III, "On the Line Geometry of a Class of Tensegrity Structures", in *Proceedings of a Symposium Commemorating the Legacy, Works, and Life of Sir Robert Stawell Ball*, University of Cambridge, UK, July, 2000.
21. Skelton, R.E. and Oliveira, M.C., *Tensegrity Systems*, Springer, 2009.
22. Guest, S., "The stiffness of prestressed frameworks: A unifying approach", *International Journal of Solids and Structures*, Vol. 43, Nos. 3–4, pp. 842–854, 2006.
23. Arsenault M., "Stiffness analysis of a 2DOF planar tensegrity mechanism", *Journal of Mechanisms and Robotics*, Vol. 3, No. 2, pp. 021011, 2011.
24. Oppenheim, I.J. and Williams W.O., "Geometric effects in an elastic tensegrity structure", *Journal of Elasticity*, Vol. 59, pp. 51–65, 2000.

APPENDIX A. ELEMENTS OF MATRICES M, F, G AND H AND ELEMENTS OF VECTOR W

It is noted that M_{ij} is the element located on the ith line and jth column of **M**, etc.

$$M_{11} = \frac{25m}{16} + \frac{m[20L^2 + 3(\rho_1+\rho_2)^2]}{48\lambda_1^2} + \frac{mL^2}{3\lambda_2^2}, \quad M_{12} = \frac{9m}{16} + \frac{m[20L^2 + 3(\rho_1+\rho_2)^2]}{48\lambda_1^2}, \tag{A.1}$$

$$M_{13} = \frac{-mL\sin\beta}{2}, \quad M_{21} = M_{22} = M_{12}, \quad M_{23} = M_{32} = 0, \quad M_{31} = M_{13}, \quad M_{33} = \frac{mL^2}{3}, \tag{A.2}$$

$$F_{11} = \frac{mL^2}{6}\left[\frac{10L^2 - \lambda_1(\rho_1+\rho_2)}{\lambda_1^5} + \frac{2\rho_1}{\lambda_2^4}\right], \quad F_{12} = \frac{mL^2}{6}\left[\frac{10L^2 - \lambda_1(\rho_1+\rho_2)}{\lambda_1^5}\right], \tag{A.3}$$

$$F_{13} = \frac{-mL\cos\beta}{2}, \quad F_{21} = F_{22} = F_{12}, \quad F_{23} = F_{31} = F_{32} = F_{33} = 0, \tag{A.4}$$

$$G_{11} = G_{21} = \frac{mL^2}{3}\left[\frac{10L^2 - \lambda_1(\rho_1+\rho_2)}{\lambda_1^5}\right], \quad G_{12} = G_{13} = G_{22} = G_{23} = G_{31} = G_{32} = G_{33} = 0, \tag{A.5}$$

$$\begin{aligned} H_{11} &= \frac{25m}{16} + \frac{c_1}{L_1^2}\left[\frac{\rho_1\lambda_2^2(\rho_1+\rho_2)}{2\lambda_1\lambda_2} - \rho_1\right]\left[\frac{\lambda_2(\rho_1+\rho_2)}{2\lambda_1} + \frac{\lambda_1\rho_1}{2\lambda_2} - \rho_1\right] \\ &\quad + \frac{c_2\rho_2^2}{4L_2^2} + \frac{c_3}{L_3^2}\left[L\cos\beta + \frac{L(\rho_1+\rho_2)\sin\beta}{\lambda_1}\right]\left[\frac{L\cos\beta - \rho_2}{2} + \frac{L(\rho_1+\rho_2)}{2\lambda_1}\right], \end{aligned} \tag{A.6}$$

$$\begin{aligned} H_{12} &= \frac{9m}{16} + \frac{c_1}{L_1^2}\left[\frac{\rho_1\lambda_1^2 - \lambda_2^2(\rho_1+\rho_2)}{2\lambda_1\lambda_2} - \rho_1\right]\frac{\lambda_2(\rho_1+\rho_2)}{2\lambda_1} + \frac{c_2\rho_1\rho_2}{4L_2^2} \\ &\quad + \frac{c_3}{L_3^2}\left[L\cos\beta + \frac{L(\rho_1+\rho_2)\sin\beta}{\lambda_1}\right]\left[\frac{-L\cos\beta - \rho_1}{2} + \frac{L(\rho_1+\rho_2)}{2\lambda_1}\right], \end{aligned} \tag{A.7}$$

$$H_{13} = \frac{c_3}{L_3^2}\left[L\cos\beta + \frac{L(\rho_1+\rho_2)\sin\beta}{\lambda_1}\right]\left[-\rho_1 L\sin\beta - \frac{L\lambda_1\cos\beta}{2}\right], \tag{A.8}$$

$$\begin{aligned} H_{21} &= \frac{9m}{16} + \frac{c_1}{L_1^2}\,\frac{\lambda_2(\rho_1+\rho_2)}{2\lambda_1}\left[\frac{\lambda_2(\rho_1+\rho_2)}{2\lambda_1} + \frac{\lambda_1\rho_1}{2\lambda_2} - \rho_1\right] + \frac{c_2\rho_1\rho_2}{4L_2^2} \\ &\quad + \frac{c_3}{L_3^2}\left[\frac{-L\cos\beta-\rho_1}{2} + \frac{L(\rho_1+\rho_2)\sin\beta}{2\lambda_1}\right]\left[\frac{L\cos\beta-\rho_2}{2} + \frac{L(\rho_1+\rho_2)}{2\lambda_1}\right], \end{aligned} \tag{A.9}$$

$$\begin{aligned} H_{22} &= \frac{9m}{16} + \frac{c_1(\rho_1+\rho_2)^2\lambda_2^2}{4L_1^2\lambda_1^2} + \frac{c_2\rho_1^2}{4L_2^2} + \frac{c_4\rho_2^2L^2\sin\beta\cos\beta}{L_4^2} \\ &\quad \times \frac{c_3}{L_3^2}\left[\frac{-L\cos\beta-\rho_1}{2} + \frac{L(\rho_1+\rho_2)\sin\beta}{2\lambda_1}\right]\left[\frac{L(\rho_2-\rho_1)\sin\beta}{2} - \frac{L\lambda_1}{2}\cos\beta\right], \end{aligned} \tag{A.10}$$

$$\begin{aligned} H_{23} &= \frac{c_3}{2L_3^2}\left[\frac{-L\cos\beta-\rho_1}{2} + \frac{L(\rho_1+\rho_2)\sin\beta}{2\lambda_1}\right]\left[\frac{L\cos\beta-\rho_2}{2} + \frac{L(\rho_1+\rho_2)}{2\lambda_1}\right] \\ &\quad + \frac{c_4\rho_2^2L^2\sin^2\beta}{L_4^2}, \end{aligned} \tag{A.11}$$

$$H_{31} = \frac{c_3}{L_3^2}\left[\frac{L(\rho_2-\rho_1)\sin\beta}{2} - \frac{L\lambda_1}{2}\cos\beta\right]\left[\frac{L\cos\beta-\rho_2}{2} + \frac{L(\rho_1+\rho_2)}{2\lambda_1}\right], \tag{A.12}$$

$$\begin{aligned} H_{32} &= \frac{c_3}{L_3^2}\left[\frac{L(\rho_2-\rho_1)\sin\beta}{2} - \frac{L\lambda_1}{2}\cos\beta\right]\left[\frac{-L\cos\beta-\rho_1}{2} + \frac{L(\rho_1+\rho_2)}{2\lambda_1}\right] \\ &\quad + \frac{c_4\rho_2 L\sin\beta}{L_4^2}(\rho_2 - L\cos\beta), \end{aligned} \tag{A.13}$$

$$H_{33} = \frac{c_3}{L_3^2}\left[\frac{L(\rho_2-\rho_1)\sin\beta}{2} - \frac{L\lambda_1}{2}\cos\beta\right]^2 + \frac{c_4\rho_2^2L^2\sin^2\beta}{L_4^2}, \tag{A.14}$$

where

$$\lambda_1 = \sqrt{4L^2 - (\rho_1+\rho_2)^2}, \quad \lambda_2 = \sqrt{L^2-\rho_1^2}. \tag{A.15}$$

The vector $\mathbf{W}$ is a 3×1 matrix whose elements are as follows:

$$W_1 = \frac{k_2L\cos\beta}{2} - k_1\rho_1 - \frac{k_1[\rho_1\lambda_1^2 - \lambda_2^2(\rho_1+\rho_2^2)]}{\lambda_1\lambda_2} - \frac{(k_2+k_4)\rho_2}{2} + \frac{k_2L(\rho_1+\rho_2)\sin\beta}{2\lambda_1} + f_1, \tag{A.16}$$

$$W_2 = k_3\rho_2 - \frac{k_2k_4\rho_1}{2} - \left(\frac{k_2}{2}+k_3\right)L\cos\beta + \frac{2k_1\rho_2\lambda_2^2(\rho_1+\rho_2^2)}{\lambda_1\lambda_2} + \frac{k_2L(\rho_1+\rho_2)\sin\beta}{2\lambda_1} + f_2, \tag{A.17}$$

$$W_3 = \frac{L\sin\beta}{2}[(k_2+2k_3)\rho_2 - k_2\rho_1] - \frac{k_2L\cos\beta\lambda_1}{2}. \tag{A.18}$$